HHS Public Access

Author manuscript

Proc SPIE Int Soc Opt Eng. Author manuscript; available in PMC 2020 March 25.

Published in final edited form as:

Proc SPIE Int Soc Opt Eng. 2020 February ; 11317: . doi:10.1117/12.2544493.

High-resolution x-ray luminescence computed tomography

Michael C. Lun, **Changqing Li***

Department of Bioengineering, University of California, Merced, Merced, CA 95343, USA.

Abstract

High-resolution imaging modalities play a critical role for advancing biomedical sciences. Recently, x-ray luminescence computed tomography (XLCT) imaging was introduced as a hybrid molecular imaging modality that combines the high-spatial resolution of x-ray imaging and molecular sensitivity of optical imaging. The narrow x-ray beam based XLCT imaging has been demonstrated to achieve high spatial resolution, even at depth, with great molecular sensitivity. Using a focused x-ray beam as the excitation source, orders of magnitude of increased sensitivity has been verified compared with previous methods with a collimated x-ray beam. In this work, we demonstrate the high-spatial resolution capabilities of our focused x-ray beam based XLCT imaging system by scanning two sets of targets, differing in the target size, embedded inside of two tissue-mimicking cylindrical phantoms. $Gd_2O_2S:Eu^{3+}$ targets of 200 μm and 150 μm diameters were created and embedded with the same edge-to-edge distances as their diameters respectively. We scanned and reconstructed a single transverse section and successfully demonstrated that a focused x-ray beam with an average dual-cone size of 125 μm could separate the targets in both phantoms with good shape and location accuracy. We have also improved the current XLCT imaging system to make it feasible for fast three-dimensional XLCT scanning.

Keywords

x-ray luminescence computed tomography; optical imaging; x-ray imaging; optical tomography; tomographic imaging

1. INTRODUCTION

Combining the merits of both x-ray imaging (high-spatial resolution) and optical imaging (high-molecular sensitivity), x-ray luminescence computed tomography (XLCT) imaging has become an attractive imaging modality for the molecular imaging of deeply embedded x-ray excitable contrast agents. In principle, XLCT imaging uses x-ray photons to excite deeply embedded contrast agents inside an object, which emit optical photons that are measured using sensitive detectors, such as a photomultiplier tube (PMT), for the tomographic reconstruction of the contrast agent distribution inside the object. The first selective-excitation based XLCT imaging system was proposed by Pratx *et al.* [1–2] and demonstrated that x-ray excitable contrast agents could be imaged with high-spatial resolution and measurement sensitivity. Soon after, many research groups, including our

*Corresponding Author: Changqing Li, Tel.: (209) 228-4777; cli32@ucmerced.edu.

own efforts, have made contributions to improve the feasibility and performance of XLCT imaging from many aspects.

XLCT imaging can be performed with several different x-ray beam geometries with the narrow x-ray beam and conical x-ray beam as the most popular choices. Selective-excitation based XLCT imaging utilizes narrow x-ray beams and can obtain very high spatial resolution, even for deeply embedded targets, due to the selective-excitation scheme. The drawback of this method is that for high-spatial resolution, a very fine x-ray beam must be used, which leads to a small excitation region and thus a long time required to scan an object. On the other hand, with the conical x-ray beam, the entire object is irradiated at one time thus the scanning times are very short. However, the x-ray beam's size and location cannot be used to aid in the reconstruction as with the narrow-beam geometry, thus we have a degraded spatial resolution in comparison. With the benefits of the selective-excitation scheme (higher spatial-resolution), we have explored several ways to improve upon existing systems to make XLCT imaging a more attractive imaging modality for small-animal imaging.

We originally explored narrow-beam XLCT imaging with a pencil x-ray beam generated from a pinhole collimator placed in front of the x-ray tube window and detected optical photons using an electron-multiplying charge-coupled device (EMCCD) camera [3–7]. With this method, we were able to separate two targets embedded inside turbid media with an edge-to-edge distance of 0.4 mm [5] and were successful in performing XLCT imaging at imaging depths larger than 2 cm with concentrations of $Gd_2O_2S:Eu^{3+}$ as low as 0.01 mg/mL [8]. We then proposed a multiple-beam scanning strategy [6] in order to decrease the imaging time. Following, we developed and built a focused x-ray beam based XLCT imaging system as described in [7]. By using a polycapillary lens to focus x-ray photons to a fine spot, we obtained much higher x-ray photon flux which allows for increased sensitivity. In addition, we demonstrated that PMTs instead of EMCCD cameras allows for an increased signal to background ratio (SBR) and shorter acquisition time during imaging.

For the spatial-resolution in the narrow-beam XLCT imaging, we have found that the key factor was the scanning x-ray beam size [5]. From our numerical simulations on the effects of the x-ray beam size on the spatial resolution, we had found that if the target separation (EtE distance) was smaller than the x-ray beam diameter, then our scanning strategy for XLCT imaging would not be able to resolve the targets. However, we recently found that if we applied a reduced step-size scanning strategy as in [9], then the spatial-resolution could be improved by 1.6 times. With our current prototype focused x-ray beam based XLCT imaging system described in [7], the x-ray tube with polycapillary lens can generate x-ray photons with a maximum x-ray beam diameter of about 150 μm (in the scanning region for the object). From our previously mentioned studies, with a typical XLCT scanning strategy, then we should be able to resolve targets separated with an EtE distance of 150 μm as well. However, in the past, a major challenge has been the fabrication of high-resolution targets that can be used for XLCT imaging, thus we have only been able to demonstrate a spatial resolution of 0.8 mm (0.4 mm EtE distance) [5, 7]. We recently have obtained even smaller glass capillary tubes which will allow us to create targets of 150 μm size in order to experimentally verify the high spatial-resolution capabilities of our XLCT imaging system.

The rest of this paper is organized as follows. In Section 2, we describe the high-resolution XLCT imaging experimental set-up including the imaging system design, phantom geometry and composition, and scanning scheme. We also discuss about some improvements we have made to that system recently in order to acquire 3D XLCT data in a reasonable time. In Section 3 of the paper we show the results of our high-resolution imaging experiments. Finally, in Section 4, we end the paper with a discussion and conclusions.

2. METHODS

2.1 High-resolution XLCT experimental set-up

We have performed two phantom experiments using two sets of targets of different sizes in order to validate the high-resolution imaging capabilities of our XLCT experimental set-up. Fig. 1 shows the overall phantom geometry used in this study. Cylindrical phantoms of 12 mm diameter and 20 mm height were created and composed of 1% intralipid, 2% agar, and water. Two sets of high-resolution targets were created using high-precision glass capillary tubes (Drummond Scientific) with O.D./I.D. of 0.40/0.20 mm and 0.30/0.15 mm, respectively. The I.D. of the capillary tubes is considered as the actual target diameter. We then mixed 10 mg/mL of GOS:Eu^{3+} (UKL63/UF-R1, Phosphor Tech. Ltd.) into a similar background solution as the phantom and injected the solution into the capillary tube targets before embedding them into the phantoms as shown in Fig. 1(b). One phantom was embedded with two targets of 0.20 mm diameter and the other phantom was embedded with the 0.15 mm diameter targets. For each phantom, the edge-to-edge (EtE) distance of the two embedded targets was the same as the target diameters (i.e. 0.20 mm and 0.15 mm EtE distances respectively).

We have performed the XLCT scans inside of our focused x-ray beam based XLCT imaging system as described in [7]. Fig. 2 below shows a computer-aided design (CAD) model of the imaging system. High-energy x-ray photons were generated by the x-ray tube (X-Beam [Mo anode], XOS) and were focused by a polycapillary lens to a focal spot of approximately 101.5 μm in a dual -cone geometry. The phantom to be imaged was placed on top of a stage that is positioned within the focal distance (~45 mm) of the polycapillary lens and the x-ray beam diameter increases to a maximum of 150 μm within the phantom scanning region with an average dual-cone diameter of 125 μm. The phantom stage sits on top of a manual lab jack (LJ750/M, Thorlabs) that allowed us to manually adjust the x-ray beam scanning depth. The jack was mounted on top of a rotary stage (B4872TS-ZR, Velmex Inc.) which was then mounted on top of a linear stage (Unislide MA40, Velmex Inc) that allowed the object to translate and rotate during imaging. An x-ray detector (Shad-o-Box 1024, Teledyne DALSA) is mounted opposite of the x-ray beam and is used to determine the object boundary during measurements. During the scan emitted optical photons from the object that reach the side surface were collected using an optical fiber bundle which is positioned as shown in Fig. 2 and delivers the photons to a fan-cooled PMT (H7422–50, Hamamatsu Inc.). The signal was sent to a broadband preamplifier (SR445A, Stanford Research Systems) with a gain of 15 and then filtered (BLP-10.7+, f_c = 11 MHz, Mini-Circuits) before being collected by a high-speed oscilloscope (MDO3104, Tektronix) and saved to a lab computer.

The entire imaging system set-up besides the amplifier, oscilloscope, and computer was fixed inside of a lead cabinet to shield from radiation and allowed for the system to be light-tight. The PMT was further shielded from the x-ray with a lead wall as seen in Fig. 2. A macro program was written in Microsoft Visual Studios to control the hardware and acquire the imaging data during the XLCT scan.

For our XLCT scans, we operated the x-ray tube at a setting of 30 kV and 0.5 mA (15 W) and took measurements from 6 angular projections (30°/projection) using 80 linear steps with a step size of 0.15 mm to traverse the whole phantom. The PMT was operated with a control voltage of 0.750 V and the oscilloscope was set to acquire or save 100 milliseconds (ms) of data from the PMT at each step. After the XLCT scan, we immediately performed a microCT scan inside of our dedicated microCT scanner described in [8] in order to determine the ground-truth location of the embedded targets for each phantom. We acquired microCT projection images from 180 projections using an angular step size of 2°. MicroCT image reconstruction was performed in MATLAB using the filtered back-projection (FBP) algorithm with a Shepp-Logan filter. For XLCT imaging, image reconstruction is similar to fluorescence molecular tomography [10]. The images of the scanned section were reconstructed using an optical photon propagation model (radiative transport equation) inside turbid media, which also included information such as the x-ray beam's known size and location to aid in the reconstruction. Here, we utilized the L^1 regularized majorization-minimization algorithm to reconstruct our XLCT images. Details of the algorithms can be found in [11–14].

2.2 Benchtop three-dimensional (3D) XLCT imaging system design

The XLCT imaging system described in Section 2.1. is currently only capable of 2D XLCT imaging since the lab jack needs to be manually adjusted by hand in order to change the scanning depth. This requires that the x-ray tube be powered off in order to safely adjust the depth and then back on for scanning which leads to unfeasible scanning times for 3D imaging. We recently have acquired new stages as upgrades to the previous XLCT imaging system, including a motorized lift which will allow us to automatically control and change the scanning depth. In short, we have added a different linear stage (NLE-100, Newmark Systems Inc.), rotary stage (RT-3, Newmark System Inc.) and lastly a motorized vertical lift (VS-50, Newmark Systems Inc.) to replace the previous stages and manual lab jack. In addition, we have fixed the optical fiber bundle, so it does not move during the image acquisition. The rest of the imaging system remains the same as before. During imaging, after a typical 2D scan, the vertical lift is programmed to then adjust the scanning depth to acquire the next 2D image and this is repeated for an inputted number of iterations and vertical step size. This system is currently being set-up in our lab and a macro program is being written in order to control the hardware and acquire images as before. We will report our progress with this set-up in the oral presentation.

3. RESULTS

Fig. 4 shows a single transverse slice from the microCT reconstruction corresponding to the XLCT scan section for both phantoms. Fig. 4(a) shows the phantom embedded with two

0.40/0.20 mm (O.D./I.D.) capillary tube targets and Fig. 4(b) shows the case with the 0.30/0.15 mm capillary tube targets. Using the microCT image, the center of the phantom was determined, and then the distance from the phantom center to the target centers was used as the ground-truth locations.

For the XLCT reconstruction, the scanned section was interpolated onto a 2D grid with a pixel size of 25 μm^2. The system matrix was interpolated onto the grid from the system matrix calculated on a finite element mesh. The results of the XLCT reconstruction for the phantom embedded with two 0.20 mm diameter targets are shown in Fig. 5. Fig. 5(a) shows the raw reconstructed image from the acquired data and Fig. 5(b) plots a zoom in on the target region (shown as a yellow box in Fig. 5(a)) with the true target locations (acquired from Fig. 4(a)) shown as green circles. We can see that two targets have been clearly resolved with good shape and location accuracy. We have calculated the DICE similarity coefficient for this reconstruction to be 78.5%. To analyze the reconstruction further, a normalized line profile plot through the center of the two targets (blue dashed line in Fig. 5(b)) is shown in Fig. 5(c) where the true target profile is indicated by a dashed black line and the reconstruction is shown as the red line. We can see good agreement between the two profile plots.

The results of the XLCT scan of the phantom embedded with two 0.15 mm diameter targets is shown in Fig. 6 as before. Again, the two embedded targets were successfully resolved and the DICE was calculated as 55.6%. Based on the normalized profile plot shown in Fig. 6(c), the two targets have been reconstructed very well.

4. DISCUSSIONS AND CONCLUSIONS

High-resolution imaging modalities play an important role for advancing biomedical sciences. Particularly, XLCT imaging has emerged as an attractive tool with various applications, for example in small-animal molecular imaging. In this work, we have performed high-resolution focused x-ray beam based XLCT imaging experiments and have demonstrated that our imaging system described in Section 2.1 can resolve two targets embedded in turbid media with EtE distances of 0.15 mm or 150 μm. This is an improvement from our previous experiments [5, 7] where we could only demonstrate imaging with targets embedded with 400 μm EtE distances. For the XLCT reconstruction of the first phantom embedded with the 200 μm targets (Fig. 5), we can see a very clear separation between the two targets which is expected as the focused x-ray beam size is much smaller than the EtE separation. When the target EtE distance decreases to 150 μm, as with the second phantom (Fig. 6), we can see that the reconstruction quality slightly degrades, as indicated by the decrease in the DICE coefficient, but the value (55.6%) is still acceptable. We anticipate that we are still able to demonstrate even higher-resolution imaging (less than 150 μm EtE) with this system, however, smaller targets are not possible to fabricate with our current resources. With our future small-animal dedicated focused x-ray luminescence tomography (FXLT) imaging system described in [15–16], we will have even higher spatial-resolution capabilities for XLCT imaging since the x-ray beam size is approximately one-half the size of the beam used in this study.

With the improvements to the imaging system as described above in Section 2.2, we can also expand our imaging capabilities to perform 3D XLCT imaging in a reasonable time. With our current set-up in Section 2.1, the manual lab-jack is a limiting factor in the ability to perform the 3D scanning due to the time required to adjust the scanning depth. With the improved vertical lift, we can accurately adjust the scanning depth with a motion controller and monitor the adjustments with an encoder. Compared with the previous stages, we have more accurate scanning step size which is important for high-resolution imaging. We also plan to incorporate a continuous scanning scheme with this imaging system. Compared with previous method of stepping through the object and acquiring our data at every step, we can take a single continuous translational step for each projection which should reduce the imaging time substantially.

In summary, in this work we have performed high-resolution XLCT imaging experiments of cylindrical phantoms embedded with two targets with EtE distances as small as 150 μm and have validated that the targets can be successfully resolved. We anticipate that we can still obtain higher spatial resolution, especially if we use a smaller x-ray beam size. The proposed high spatial-resolution XLCT imaging system with such unique imaging capabilities would have many applications, such as for studying tumor microenvironment (e.g. oxygenation) or structure. In addition, we have also improved the current XLCT imaging system which allows for more feasible 3D XLCT with reduced scan time. We will plan to demonstrate high-resolution 3D XLCT imaging in the future studies.

ACKNOLWEDGMENTS

This work is funded by the NIH National Institute of Biomedical Imaging and Bioengineering (NIBIB) [R01EB026646].

REFERENCES

[1]. Pratx G, Carpenter CM, Sun C, Rao R, and Xing L, “Tomographic molecular imaging of x-ray excitable nanoparticles,” Opt. Lett 35, 3345–3347 (2010). [PubMed: 20967061]

[2]. Pratx G, Carpenter CM, Sun C, and Xing L, “X-ray Luminescence Computed Tomography via Selective Excitation: A Feasibility Study,” IEEE Trans. Med. Imag 29 (12), 1992–1999 (2010).

[3]. Li C, Di K, Bec J, and Cherry SR, “X-ray luminescence computed tomography imaging: experimental studies,” Opt. Lett 38, 2339–41 (2013). [PubMed: 23811921]

[4]. Li C, Martinez-Davalos A, and Cherry SR, “Numerical simulation of x-ray luminescence computed tomography for small-animal imaging,” J. Biomed. Opt 19, 046002 (2014). [PubMed: 24695846]

[5]. Zhang W, Zhu D, Lun M, and Li C, “Collimated superfine x-ray beam based x-ray luminescence computed tomography,” J. X-ray Sci. Technol 25 (6), pp 945–957, (2017).

[6]. Zhang W, Zhu D, Lun M, and Li C, “Multiple pinhole collimator based x-ray luminescence computed tomography,” Biomed. Opt. Expr 7 (7), 2506–23 (2016).

[7]. Zhang W, Lun MC, Nguyen A, and Li C, “A focused x-ray beam based x-ray luminescence computed tomography,” J. Biomed. Opt 22 (11), 116004 (2017).

[8]. Lun MC, Zhang W, and Li C, “Sensitivity study of x-ray luminescence computed tomography,” Appl. Opt 56 (11), 3010–3019 (2017). [PubMed: 28414356]

[9]. Zhang Y, Lun MC, Li C, and Zhou Z, “Method for improving the spatial resolution in narrow x-ray beam based x-ray luminescence computed tomography,” J. Biomed. Opt 24 (8), 086002 (2019).

[10]. Li C, Mitchell GS, Dutta J, Ahn S, Leahy RM, and Cherry SR, "A three-dimensional multispectral fluorescence optical tomography imaging system for small-animals based on a conical mirror design," Opt. Expr 17 (9), 7571–7585 (2009).

[11]. Zhu D, Zhao Y, Baikejiang R, Yuan Z, and Li C, "Comparison of regularization methods in fluorescence molecular tomography", Photonics, 1, 95–109 (2014).

[12]. Zhu D and Li C, "Nonconvex regularizations in fluorescence molecular tomography for sparsity enhancement," Phys. Med. Biol 59, 2901–2912 (2014). [PubMed: 24828748]

[13]. Zhu D and Li C, "Nonuniform update for sparse target recovery in fluorescence molecular tomography accelerated by ordered subsets," Biomed. Opt. Express 5, 4249–4259 (2014). [PubMed: 26623173]

[14]. Zhu D and Li C, "Accelerated image reconstruction in fluorescence molecular tomography using a non-uniform updating scheme with momentum and ordered subsets methods," J. Biomed. Opt 21, 016004 (2016).

[15]. Lun MC and Li C, "Focused X-ray Luminescence Computed Tomography," Proc. SPIE 11113, Developments in X-Ray Tomography XII, 111131B (2019).

[16]. Lun MC, Cong W, Arifuzzaman M, Ranasinghe M, Bhattacharya S, Anker J, Wang G, and Li C, "X-ray luminescence imaging for small-animals," Proc. SPIE 11224, Optics and Ionizing Radiation, (In Press).

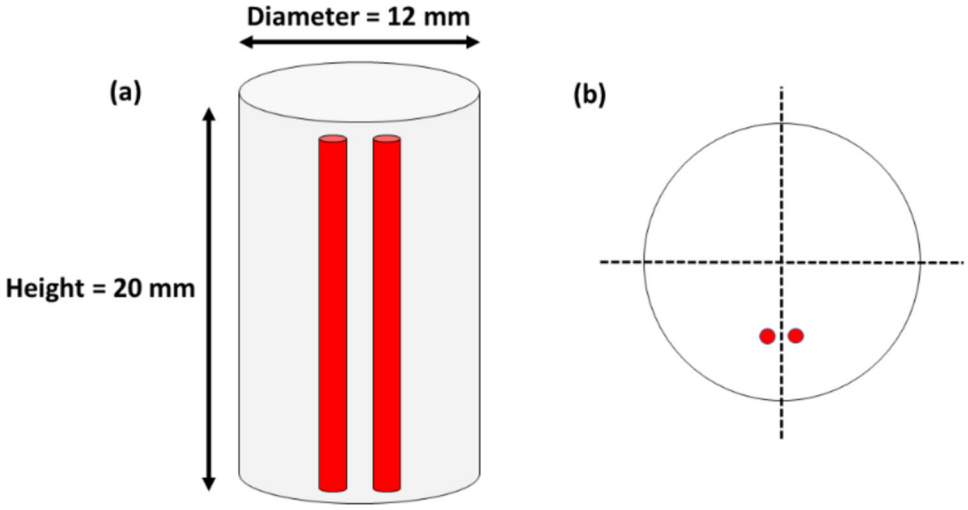

Figure 1.
Schematic phantom geometry for high-resolution XLCT imaging experiments. (a) Overall phantom geometry; (b) Top-view showing embedded target location.

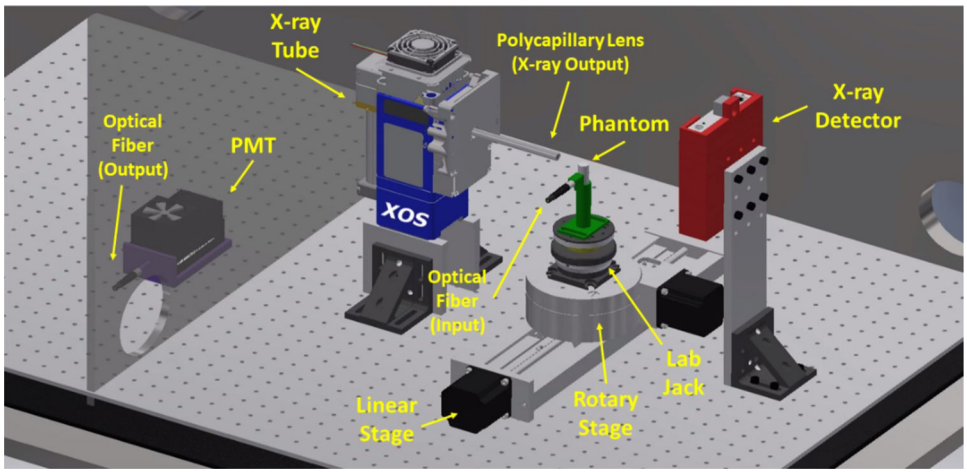

Figure 2.
CAD model of the focused x-ray beam based XLCT imaging system.

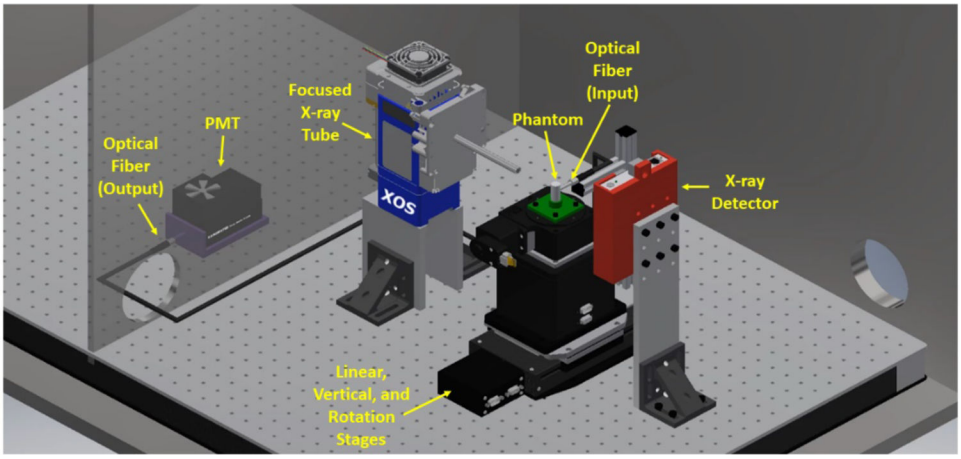

Figure 3.
CAD model of upgraded 3D focused x-ray beam based XLCT imaging.

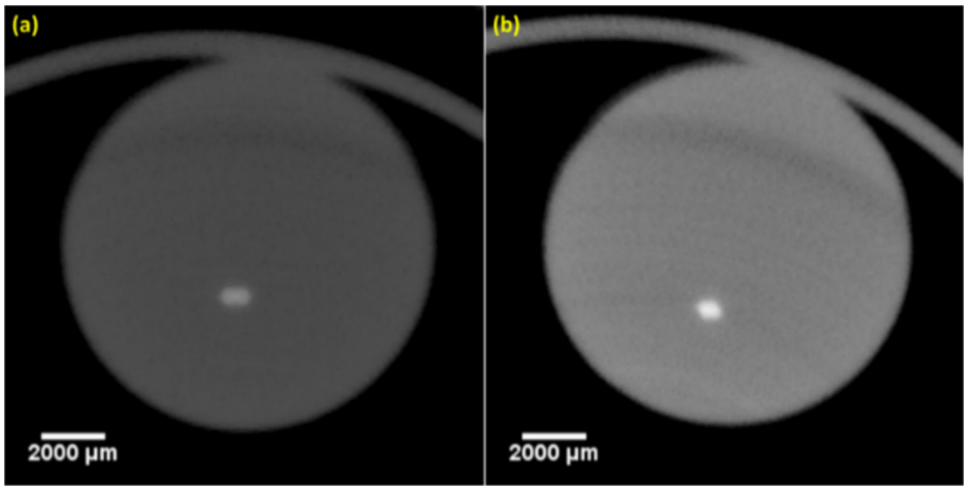

Figure 4.
microCT image of phantoms used in high-resolution XLCT imaging experiments. (a) Phantom embedded with 0.20 mm diameter targets; (b) Phantom embedded with 0.15 mm diameter targets.

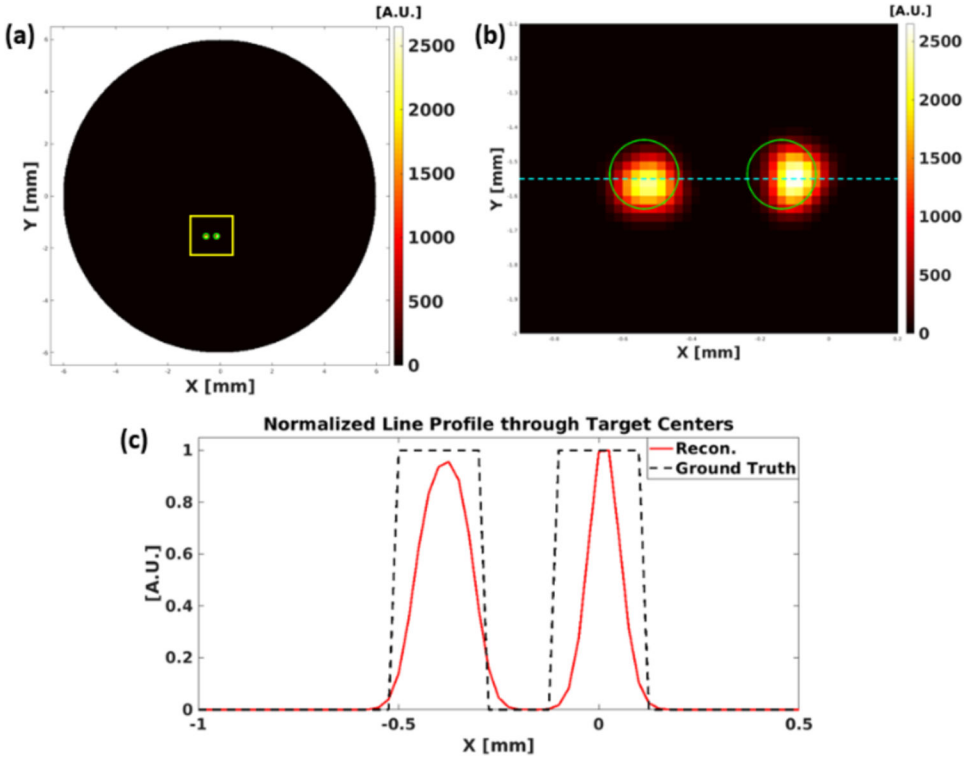

Figure 5.

XLCT reconstruction of phantom embedded with 0.2 mm (200 μm) diameter targets. (a) XLCT reconstructed image; (b) Zoomed-in target region (yellow box in (a)); (c) Normalized line intensity plot (blue line in (b)).

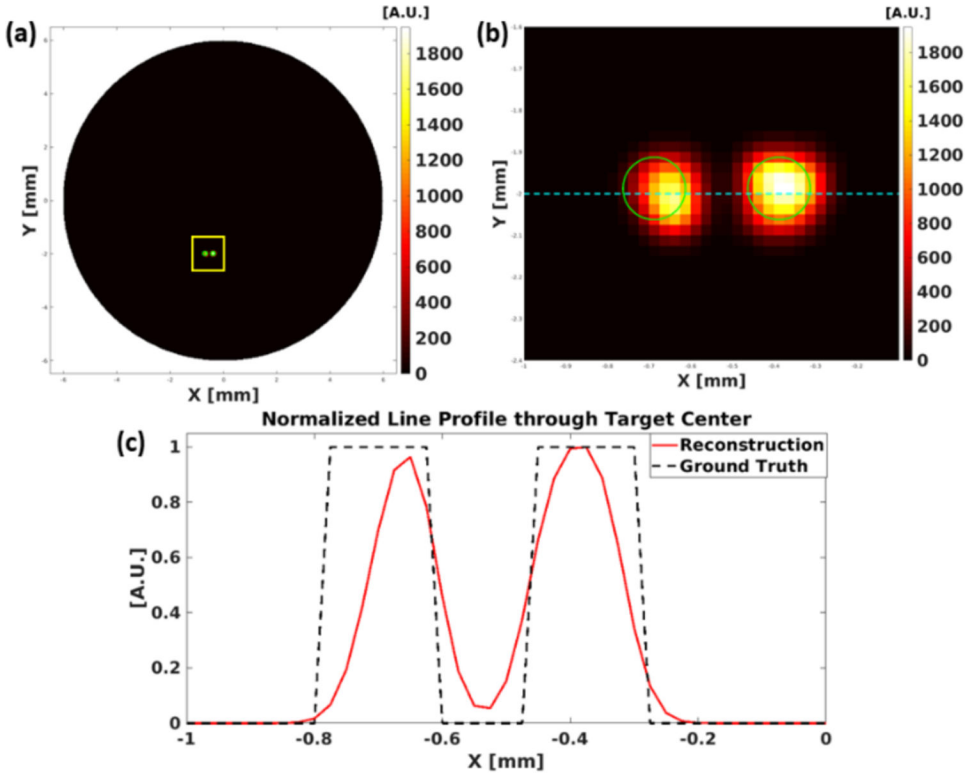

Figure 6.

XLCT reconstruction of phantom embedded with 0.15 mm (150 μm) diameter targets. (a) XLCT reconstructed image; (b) Zoomed-in target region (yellow box in (a)); (c) Normalized line intensity plot (blue line in (b)).